This is a preprint, the final version is subject to change, of the American Mineralogist (MSA)
Cite as Authors (Year) Title. American Mineralogist, in press.
DOI: https://doi.org/10.2138/am-2020-7216

Revision 2

An experimental approach to examine fluid-melt interaction and mineralization in rare-metal pegmatites

Alysha G. McNeil[1], Robert L. Linnen[1], Roberta L. Flemming[1], and Mostafa Fayek[2]

[1] *Department of Earth Sciences, Western University, 1151 Richmond Street North, London, ON N6A 5B7, Canada*

[2] *Department of Geological Sciences, University of Manitoba, 240 Wallace Building, 125 Dysart Road, Winnipeg, MB R3T 2N2, Canada*

Abstract

Niobium and tantalum, rare metals and high field strength elements (HFSEs) that are essential to modern technologies, are concentrated among others in Lithium-Cesium-Tantalum (LCT) pegmatites and rare metal granites. The most important hosts for Nb-Ta in these types of deposits are the columbite group minerals (columbite-tantalite), but at some ore deposits significant Ta is also contained in wodginite, microlite and tapiolite. Previous solubility experiments of HFSE minerals have been limited to high temperatures because of the slow diffusivities of HFSEs in granitic melts. An experiment protocol is described herein that allows HFSE mineral solubilities to be determined at lower temperatures, more in line with the estimated solidus temperatures of LCT pegmatites and rare metal granites. This is achieved through the interaction of a melt that is enriched in high field strength elements (e.g., P and Nb or Ta) with a fluid enriched in a fluid mobile element (FME, e.g., Mn). A starting glass enriched in a slow diffusing HFSE was synthesized and HFSE mineral saturation is obtained via the diffusion of a FME into the melt via interaction with a fluid. This interaction can occur at much

lower temperatures in reasonable experimental durations than for experiments that require diffusion of niobium and tantalum. The solubility product of columbite-(Mn) from the fluid-melt interaction experiment in a highly fluxed granitic melt at 700 °C is the same as those from dissolution and crystallization (reversal) experiments at the same P-T conditions. Thus, both methods produce reliable measurements of mineral solubility and the differences in the metal concentrations in the quenched melts indicates that the solubility of columbite-(Mn) follows Henry's Law. Results show that columbite-(Mn) saturation can be reached at geologically reasonable concentrations of niobium in melts and manganese in hydrothermal fluids. This experimental protocol also allows the investigation of HFSE mineral crystallization by fluid-melt interactions in rare-metal pegmatites. Magmatic origins for columbite group minerals are well constrained but hydrothermal Nb-Ta mineralization has also been proposed for pegmatite-hosted deposits such as Tanco, Greenbushes, and granite-hosted deposits such as Cínovec/Zinnwald, Dajishan and Yichun. This study shows that columbite-(Mn), lithiophilite and a Ca-Ta oxide mineral that is likely microlite crystallized from experiments in fluid-melt systems at temperatures as low as 650 °C at 200 MPa. It is important to note that HFSE minerals that crystallize from fluid-melt interactions texturally occur as euhedral crystals as phenocrysts in glass, i.e., are purely magmatic textures. Therefore, crystallization of HFSE minerals from fluid-melt interactions in rare metal granites and pegmatite deposits may be more widespread than previously recognized. This is significant because the formation of these deposits may require magmatic-hydrothermal interaction to explain the textures present in deposits worldwide, rather than always being the result of a single melt or fluid phase.

Keywords: experimental petrology, rare metals, pegmatite, niobium, fluid-melt interactions

Introduction

Niobium and tantalum are commonly referred to as 'geochemical twins' due to their similar physical and chemical properties, and owing to their importance to society, they are classified as critical elements (Graedel et al. 2015). Niobium is used in high-strength, low-alloy steel, and MRI and NMR instruments; Ta is used by the electronics industry because of its ability to store and release energy, which is critical to the miniaturization of electronic components (Schulz and Papp 2014). Most of the world's niobium production is from carbonatite complexes, although Nb resources are also associated with alkaline complexes (Mackay and Simandl 2014). The main ore minerals in these associations are pyrochlore group and columbite group minerals (CGM). The most important sources of Ta are rare-metal granite- and pegmatite-hosted deposits (Linnen, Trueman and Burt 2014), where Nb-Ta resources are dominantly from CGMs. Tantalite (a CGM) is the most common Ta mineral, but wodginite and microlite also host significant amounts of Ta at some deposits. Table 1 summarizes the characteristics of different deposit types that host Nb/Ta minerals, and these characteristics are further explained below.

The solubilities of CGMs in melts and magmatic origins are well constrained (Keppler 1993; Linnen and Keppler 1997; Linnen 1998; Bartels et al. 2010; Chevychelov et al. 2010; Van Lichtervelde et al. 2010; Fiege et al. 2011, 2018; Aseri et al. 2015; Tang et al. 2016; McNeil et al. 2019). These experiments show that temperature and melt composition (ASI, molar Al/(Na+K) and ASI_{Li}, molar Al/(Li+Na+K)) are the most important controls on magmatic CGM crystallization. Current explanations for magmatic CGM crystallization either take into account the slow diffusivity of Nb and Ta in fluxed boundary layers and propose that metals are concentrated via zone refinement (London 2008, 2018), or invoke metal enrichment through immiscible liquids (Thomas and Davidson 2016). However, in both cases Nb and Ta are

enriched in the melt, and not in coexisting aqueous fluid (Borisova et al. 2012) and the mechanism of CGM deposition is not clear.

It has been long recognized that metasomatism (alteration involving the introduction and/or removal of chemical components from the interaction of a rock with aqueous fluids) can take place in rare-metal granites (e.g. Schwartz 1992) and albitization and greisenization (hydrothermal alteration of feldspar and muscovite by a fluorine-rich fluid) are identified in LCT pegmatites (e.g. Černý 1986). Studies on natural LCT pegmatites or granites (e.g., Partington et al. 1995; Černý 2005; Rao et al. 2009; Breiter et al. 2017; Wu et al. 2017, 2018) propose that hydrothermal processes are important to the crystallization of Nb and Ta minerals. In fact, some of the highest grades of Ta mineralization within the Tanco pegmatite are hosted by zones of replacement-style muscovite-quartz after microcline (MQM) (Van Lichtervelde et al. 2007). An additional observation is that the mineralogy associated with metasomatism is complex and involves the intergrowths of several different Ta-bearing phases (Van Lichtervelde et al. 2007). It is important to note that these authors proposed that a possible explanation for this complex, metasomatic style of mineralization is that it took place at the stage where fluids and melts co-existed and fluids could have transported mineral constituent elements (Mn, Fe and Sn) to Ta-rich melts to crystallize magmatic Ta minerals. This has yet to be tested experimentally, although Cheng et al. (2019) propose that tourmaline concentrated at the roofs of granite intrusions may be the result of "self-metasomatism" where boron-rich fluids interact with magma. In the environment of coexisting melt and fluid the ore minerals can be considered to consist of dominantly magmatic elements (HFSE such as Nb and Ta) and elements that are potentially more mobile (fluid mobile elements, FME, such as Mn, Fe, Sn and Ca). Although all elements can be considered fluid mobile depending on the composition of the fluid and P-T, HFSEs such

as niobium and tantalum have very low solubilities in hydrothermal fluids at near-neutral pH conditions, i.e., buffered by the coexistence of feldspars and micas and the available experimental data indicate that the fluid-melt partition coefficients of Nb and Ta are very low (e.g., Borodulin et al. 2009). This is consistent with the lack of Ta haloes around most rare metal granites and LCT pegmatites (e.g., Cuney et al. 1992). Niobium and tantalum can be transported by fluorine-rich fluids at low pH (Borodulin et al. 2009; Zaraisky et al. 2010; Tang et al. 2015; Timofeev et al. 2015, 2017), but this is inconsistent with the coexistence of feldspars and muscovite in most LCT pegmatites and rare metal granites. Immiscible peralkaline melt fractions have been suggested as a potential method for mobilization of Nb and Ta (Thomas et al. 2011; Müller et al. 2018). Niobium transport at high pH is consistent with the observed metasomatic haloes around alkaline intrusions (fenites, which are related to alkaline fluids). By contrast, FMEs such as Ca and Mn are readily complexed by chlorine-bearing magmatic fluids (Webster and Holloway 1988; Zajacz et al. 2008). Such fluids could provide Mn or Fe to the site of CGM deposition. Some LCT pegmatites (e.g. S-type peraluminous granites and pegmatites) are already rich in Mn, as exampled by the presence of spessartine (Maner et al. 2019), however in other pegmatites and granites, particularly those that have been exploited for Ta, e.g., Tanco, Canada (e.g. Anderson 1992, Černý, 2005), Greenbushes and Wodgina, Australia (Fetherston 2004) or Yichun, China (Yin et al. 1995), spessartine is a rare to minor phase. The dominant Mn phase at these latter locations can be a Mn-phosphate such as lithiophilite or as Mn substitution in a silicate phase such as muscovite or tourmaline, together with tantalite (Van Lichtervelde et al., 2006).

The current study describes an experimental method designed to test the hypothesis of whether Nb and Ta minerals can crystallize through diffusion of Mn from a fluid into a Ta- or

Nb-rich melt in LCT pegmatites or rare-metal granites, i.e., Nb or Ta phase crystallization from a FME in a hydrothermal fluid and a magmatic HFSE. This interaction of a HFSE melt with a FME fluid will henceforth be referred to as "fluid-melt interaction(s)". To the knowledge of the authors, this type of fluid-melt interaction experiment has never been applied to study CGM or rare-metal crystallization or their solubilities. At the temperatures investigated in these experiments (650 °C to 700 °C) the H_2O-rich fluid in these experiments is likely a volatile phase that coexisted with a silicate melt (Sowerby and Keppler 2002) and will hereafter be referred to as the "fluid". This technique opens the possibility of conducting solubility experiments at lower temperatures than was previously possible because tantalum and niobium are not required to diffuse to obtain saturation. Only the FME cations need to diffuse into the melt, which can occur at much lower temperatures in reasonable experimental durations than for HFSEs with slow diffusivities such as niobium and tantalum. Columbite-(Mn) [$MnNb_2O_6$], a Ta-rich mineral assumed to be microlite and lithiophilite [$LiMnPO_4$] crystallized in these experiments and the solubility product of columbite-(Mn) and lithiophilite were determined. The solubility product of columbite-(Mn) was confirmed to be an equilibrium value by comparing results from fluid-melt interaction experiments with data from dissolution and crystallization experiments and the reproducibility of results.

Experimental procedure

The solubility of columbite-(Mn) can be defined by a solubility product (K_{sp}^{col}), i.e., $K_{sp}^{col} = [MnO] \times [Nb_2O_5]$), where [MnO] and [$Nb_2O_5$] are the concentrations of [MnO] and [Nb_2O_5] in the melt (for a more complete thermodynamic discussion see Keppler, 1993; Linnen and Keppler, 1997; McNeil et al. 2019). In order to evaluate whether the solubility products represent equilibrium values, equilibrium needs to be approached from different directions. In

dissolution experiments equilibrium is approached from undersaturation. The solubility products are obtained by dissolving columbite-(Mn) crystals in the melt. One of the criteria for equilibrium is that the results are reproducible, consequently repeat dissolution experiments were carried out at the same temperature and pressure to establish reproducibility. In crystallization experiments equilibrium is approached from oversaturation. In these experiments columbite-(Mn) was first dissolved at high temperature, then temperature was lowered, and equilibrium was approached by crystallization. If solubility product values from dissolution and crystallization experiments are in agreement, they are considered to represent equilibrium values. These experiments were completed to establish equilibrium solubility products to which the fluid-melt interaction solubility experiments (diffusion of Mn from a fluid into a Nb-doped melt) can be compared. Fluid-melt interaction experiments were designed to crystallize columbite-(Mn) from more geologically reasonable melt compositions than previous solubility experiments have allowed – with lower concentrations of Nb, in this case, 5000 ppm, and higher concentrations of Mn. It is also important to note that by definition, the concentrations of Mn and Nb can be very different and yet be saturated in columbite-(Mn). Thus, contrary to London (2018), it does not matter whether one of the elements is buffered, e.g., Mn by spessartine. To evaluate columbite-(Mn) saturation the concentrations of Mn and Nb in the melt, temperature and melt composition must all be known.

Experiment Apparatus

Experiments in this study are completed in rapid quench cold seal pressure vessels (CSPVs) that are operated vertically (see Matthews et al. 2003). Temperature was measured using an external Ni-CrNi thermocouple (error of approximately 1 °C) that was calibrated against two internal thermocouples, one measuring temperature at the top of the inside of the

autoclave, and one 3 cm from the top – the area in which capsules are placed. The internal thermocouples established that the temperature gradient in these autoclaves where capsules are placed at 650– 850 °C and 200 MPa (H_2O pressure medium) was typically less than 10 °C. Pressure was measured by transducers and results were checked against a pressure gauge. Both the transducers and gauge are factory calibrated with an accuracy of better than ±10 MPa. All experiments were conducted at fO_2 of approximately Ni-NiO. Oxygen fugacity was not directly controlled in these experiments, however the CSPVs are constructed of Udimet 720® Ni alloy with intrinsic fO_2 near Ni-NiO (Matthews et al. 2003).

Starting Glass

The starting glasses for the dissolution, repeat and crystallization experiments is a Mn-, Ta- and Nb-free hydrous glass (PEGA-H1, Table 2). The starting glasses for the fluid-melt interaction experiments were prepared by mixing batches of approximately 350 mg of anhydrous PEGA glass (Table 2) with the desired amount of Nb_2O_5 or Ta_2O_5, to produce a composition with ~5000 ppm niobium or tantalum (Table 2, NBD-5000ppm and TAD-5000ppm). This was then mixed by hand under acetone in an agate mortar for approximately 30 minutes to ensure homogeneity. The mixtures were sealed in clean, annealed gold capsules (length 30, i.d. 4.8, o.d. 5.0 mm), along with approximately 35 µL Nanopure™ water (resistivity = 18.2 MΩ) to hydrate the glasses and then run in CSPVs for seven days at 850 °C and 200 MPa. Capsules were then rapidly quenched to produce a homogeneous glass. The starting glasses were designed to be water undersaturated based on a previous study which indicates that flux-rich melts can contain up to approximately 10 wt% water at 200 MPa (Holtz et al. 1993). Therefore, the experiments would first reach saturation upon the addition of the hydrothermal fluid to the glass. Capsules were weighed to ensure no loss during the experiment due to holes in the capsule wall. Capsules

were then opened and glasses ground under acetone for another 30 minutes with a witness chip saved for analysis (Table 2).

Starting hydrothermal fluid

The composition of the hydrothermal fluid was designed to contain similar molar ratios of the alkalis present in the anhydrous starting glass (2:1 Na:K) so that the alkali ratio of the melt will be close to equilibrium. The stock fluid contained NaCl + KCl and not HCl as HCl alters the alumina saturation index (ASI) of the melt by removing sodium and adding potassium (Frank et al. 2003). The desired manganese concentration for solution was 1% Mn as $MnCl_2$. Starting chlorides were purchased from Alfa Aesar with purities of: NaCl – 99.998%; KCl – 99.997%; and $MnCl_2$ – 99.99%. A stock solution of approximately 6% NaCl + KCl (Table 3) was made by measuring out the necessary amounts of NaCl and KCl and heating them in a drying oven at 150 °C for 1 hour to ensure any absorbed water was removed. The NaCl and KCl was then added to the desired amount of ultrapure water. The water was purified using a Milli-Q® Advantage 10 Integral water purification system with a Q-POD® Element unit at the GEOMETRIC Laboratory at Western University. The water produced has a resistivity of 18.2 MΩ and is free of trace impurities such as metals or bacteria to the ppt level. It is particularly important that the stock water have concentrations of Ca and Mn as low as possible. The NaCl + KCl mixture was stirred for 30 minutes to ensure complete dissolution and homogeneity. This stock solution was then used to make the fluid for experiments by adding the desired amount of $MnCl_2$ to a small batch of stock solution and mixing the solution for 15 minutes to achieve the desired concentration. The $MnCl_2$ was purchased ultradry and ampouled under argon. The $MnCl_2$ was added to the stock solution immediately after opening the ampoule to ensure no absorbed water influenced the weight of the measured chlorides. Samples were analyzed by inductively coupled plasma mass

spectrometry (ICP-MS) at the Analytical Services Laboratory in the Western University Biotron Experimental Climate Change Research facility in London, Ontario, Canada. Samples were diluted and then filtered (0.45 um) and analyzed directly on an Agilent 7700x quadrupole ICP-MS using the helium collision cell and calibrated to aqueous standards in 2% nitric acid.

Dissolution and Crystallization Experiments

Gold tubing for capsules (o.d. 2.9 mm, i.d. 2.6 mm, 15 mm length) was cleaned by boiling in 38% HCl diluted 5:1 with deionized water, and then cleaned with acetone to remove any organic residue and annealed at 600 °C for 15 minutes. Bottoms of the capsules were welded, and then the capsules were filled with 2 mg NanopureTM water (resistivity = 18.2 MΩ) and a mixture of 30 mg hydrous PEGA-H1 glass and 3 mg of synthetic columbite-(Mn) from McNeil et al. (2015). The minerals were thoroughly mixed with the glasses by hand to not crush the crystals prior to addition to the capsule and to ensure equal distribution. The capsules were then sealed using a micro-spot arc welder and placed in an oven at 110 °C for 20 minutes to check for leaks. Any capsule exhibiting weight loss after heating was discarded. Sealed capsules were then placed in rapid quench CSPVs at 700°-850 °C and 200 MPa for 5 to 10 days. The reverse (crystallization) experiment was first run for 5 days at 850 °C, then cooled to 700 °C and left for another 5 days (10 days total) to approach equilibrium from the reverse direction (crystallization). After the desired run duration, the experiments were rapidly quenched and after removal from the CSPV, the capsules were re-weighed to ensure no weight loss over the duration of the experiment. The capsules were then opened, and representative glass chips were made into epoxy mounts for analysis by scanning electron microscope (SEM) and field emission electron probe microanalysis (FE-EPMA).

Fluid-Melt Interaction Experiments

Gold tubing for capsules were prepared as described above, then filled with 10 μL of a 2.3 wt% $MnCl_2$-bearing fluid (Table 3) and 20 mg Nb- or Ta-doped hydrous glass (Table 2). The capsules were sealed using a micro-spot arc welder, placed in an oven at 110 °C for 20 minutes and checked for leaks. Experiments were run in rapid quench cold seal pressure vessels at 650, 675 or 700 °C and 200 MPa for 5 days. After rapid quench the capsules were then re-weighed to check for weight loss and any experiments exhibiting weight loss were discarded. Upon opening, all capsules contained glass coexisting with remaining fluid within the capsule, demonstrating that fluid and melt coexisted throughout the duration of the experiments. The amount of fluid remaining in the capsule was not enough to collect for analysis but the composition can be inferred to be similar to the starting composition, however some element exchange between the melt and fluid occurred (e.g. Mn diffusion into the glass, and Li loss to the fluid). Representative glass chips were mounted in epoxy and analyzed by scanning electron microscope (SEM), field emission electron probe microanalysis (FE-EPMA), Raman spectroscopy, micro X-ray diffraction (μXRD), and Secondary Ion Mass Spectrometry (SIMS).

Analytical Methods

μX-ray diffraction

Select experiments were analyzed by μXRD in the Department of Earth Sciences at Western University using a Bruker D8 Discover X-ray microdiffractometer (Flemming 2007) with a Co Kα X-ray source (λ = 1.7902 Å) at 35 kV and 45 mA. A Göbel mirror parallel optics system was used with a 300 μm pinhole snout. The theta-theta instrument allowed samples to remain stationary and horizontal while the source and detector were set to the desired θ1+θ2=2θ, where θ1≠θ2 in omega scan mode. Omega scan parameters utilized were θ1=14.5°, θ2=22°,

ω=10°, 20-minute duration for frame one, and θ1=35.5°, θ2=40°, ω=18°, 35-minute duration for frame two. Omega scans allow for more reflections to be collected as source (θ1) and detector (θ2) both rotate clockwise, moving through omega angle ω throughout the scan, instead of the need for the sample to rotate. Results were processed from General Area Detector Diffraction System (GADDS) images using DIFFRACplus™ Evaluation software (EVA). Phases were confirmed using the International Centre for Diffraction Data Powder-Diffraction File (ICDD PDF4+ 2016) database.

Electron probe microanalysis

Major and trace elements of run products and starting glasses were analyzed using a JEOL JXA-8530F field-emission electron microprobe at the Earth and Planetary Materials Analysis Laboratory at Western University. Probe conditions for glass analyses were 20 kV accelerating voltage and 2 nA current using wavelength-dispersive spectroscopy (WDS) detectors, with a beam size of ~20 μm in order to prevent sodium migration and water loss during analyses (Morgan and London 1996). Analysis counting times were 30 seconds on peak positions and 15 seconds on each upper and lower background for major elements (Si, Na, Al, K, F, P) and 60 seconds on peak positions and 30 seconds on backgrounds for trace elements (Nb, Ta, Mn, Ca, Cl). Mineral calibration standards used were pure tantalum wire for Ta (99.996%, Alfa Aesar, USA); pure manganese for Mn (99.99%, Johnson Matthey Chemicals, UK); pure niobium wire for Nb (99.96%, Alfa Aesar, USA); Amelia albite for Na; synthetic fluorite for F; basaltic glass (Smithsonian USNM 113498/1 VG-A99 - Juan de Fuca Ridge) for Ca; rhyolite glass for Si and K (Smithsonian USNM 72854 VG-568 - Yellowstone National Park, WY); apatite for P (Wilberforce, Ontario, Canada); sodalite for Cl (Geller MicroAnalytical); and Patino glass 3 for Al (Patino-Douce et al. 1994). Due to the low concentration of niobium and tantalum

in starting glasses, a two-step analysis method was used. Major elements were first analyzed using the conditions described above, and then niobium and tantalum were analyzed at 15 kV accelerating voltage and 20 nA current, with a beam size of ~20 μm using WDS detectors, to minimize the amount of glass that would be ablated from the analysis. Analysis counting times were 60 seconds on peak positions and 30 seconds on each upper and lower background. Mineral calibration standards used for these analyses were pure tantalum wire for Ta (99.996%, Alfa Aesar, USA) and pure niobium wire for Nb (99.96%, Alfa Aesar, USA). Analysis of niobium and tantalum using this two-step method yielded the same average concentration but with enhanced precision compared to analysis using the first, original low probe current conditions, and analyses of all experiment run products were completed using the single-step analysis method. Columbite-(Mn) in successful experiments was analyzed to confirm mineral chemistry and conditions used were 15 kV accelerating voltage and 20 nA current with an ~1 μm beam using WDS detectors. Mineral calibration standards used were pure niobium wire for Nb (99.96% Alfa Aesar, USA) and pure manganese for Mn (99.99%, Johnson Matthey Chemicals, UK). As the grains were very small (≤ 1 μm), Si and P were analyzed to determine the amount of glass or lithiophilite interference in the analysis. Back scattered electron (BSE) images were taken using the SEM on the microprobe.

Raman spectroscopy

Raman spectroscopy was used to identify the manganese phosphate mineral that crystallized, which was determined to be lithiophilite [$LiMnPO_4$]. Raman analyses were completed at Surface Science Western in London, Ontario, Canada on a Renishaw inVia Reflex Raman Spectrometer using a 514 nm laser, 1800 I/mm grating, 8 milliwatts power and 50x microscope objective. Spectra of columbite-(Mn) were also collected in successful fluid

299 experiments to confirm columbite-(Mn) crystallization. Phase ID was determined by comparison
300 to reference spectra in the RRuff database. Lithiophilite and glass spectra were collected at 100%
301 power for 10 seconds, and columbite-(Mn) at 100% power for 5 seconds due to the intense signal
302 produced by columbite-(Mn) crystals.

303 **Secondary ion mass spectrometry**

304 Secondary ion mass spectrometry (SIMS) analyses of lithium and boron were completed
305 at the Manitoba Institute for Materials, University of Manitoba, Canada on a Cameca IMS 7f
306 secondary ion mass spectrometer. The crystallization of lithiophilite and anorthoclase in
307 experiments affected the lithium and boron concentrations so that the assumption that these
308 concentrations are nearly identical to that of the starting glass is no longer valid. Knowing the
309 concentration of lithium in the experiments is necessary for the calculation of ASI_{Li} (which
310 affects columbite-(Mn) solubility) and an accurate understanding of experiment properties and
311 solubilities. Lithium and boron concentrations were calculated by determining their abundance
312 relative to silicon, which is known from FE-EPMA analysis of the sample. Prior to SIMS
313 analyses, the sample and standards were cleaned by submersing the samples in an ultrasonic
314 cleaner for four separate cleaning stages. The duration of each stage was ten minutes. The liquid
315 the sample was submersed in for each stage was: dilute soap solution, tap water, distilled water,
316 and ethanol. After this process samples and standards were gold coated to ensure a conductive
317 surface. A +2 nA primary beam of O- ions was accelerated at -12.5 kV and focused to a ~15 μm
318 spot. To help shape the beam, a 750 μm aperture was used in the primary column. The sample
319 was held at +10 kV with a 0 V sample offset, and a mass resolving power of 1000 was used to
320 resolve isobaric interferences (Burdo and Morrison 1971). The detector is an ETP 133H electron
321 multiplier and analysis of 6Li+, 10B+, 30Si+ was conducted over 30 cycles with 1 second of

detection for each isotope per cycle. A 20 second pre-sputter was used to remove the gold coating and allow the secondary ion signal to stabilize on the chosen spot before analysis. Accurate analysis depends on having standard calibration in similar material to the sample being analyzed. Due to an unnatural $^{7}Li/^{6}Li$ ratio of approximately 40 in the starting $LiPO_4$ reagent (Qi et al. 1997), only one standard could be used for calibration (PEGA starting material), as other glass standards have a natural ratio of approximately 12 (Choi et al. 2013) and are not suitable to use for calibration. Boron standards used for calibration were NIST SRM 610 (Pearce et al. 1997) and PEGA from this study.

Results

Run products

Four columbite-(Mn) dissolution, one repeat, and one crystallization (reversal) experiment were completed in a highly evolved flux-rich granitic melt to compare with the solubility product of columbite-(Mn) from the fluid-melt interaction experiments. The only phases identified in dissolution experiments were columbite-(Mn) and glass. The experiments represent equilibrium because the solubility products of forward and reverse experiments are identical within error, the glass composition is homogeneous, and the Mn/Nb ratios of the glasses are approximately 0.5 (Table 4).

All Nb fluid-melt interaction experiments (Table 4) crystallized columbite-(Mn) (confirmed by Raman analyses) as thin laths up to 5 μm long and less than 1 μm wide (Figure 1). The small sizes caused minor interference from the background glass during FE-EPMA, which resulted in low Nb_2O_5 + MnO totals, but the chemical formula calculated from the average MnO and Nb_2O_5 concentrations is $Mn_{1.00}Nb_{2.00}O_6$ (Table 5).

Equant lithiophilite [$LiMnPO_4$] crystals 1 to 5 μm across (Figure 1, 2, 3) were identified through a combination of FE-EPMA-WDS and Raman spectroscopy, and crystallized in all fluid-melt interaction experiments. All experiments completed at temperatures below 700 °C also crystallized anorthoclase ($Na_{0.62}K_{0.36}Al_{1.04}Si_{2.97}O_8$, Figure 1, 2), confirmed by μXRD and FE-EPMA-WDS. As anorthoclase and lithiophilite crystallized, and Li and B were likely partitioned into the fluid phase (London et al. 1988), the experiment melt composition had changed (elements exchanged between the melt and the fluid). Therefore, it was necessary for the Li and B, contents of the glass of these experiments to be determined for both lithiophilite solubility product calculations and determination of melt/fluid exchange, and this was completed by SIMS (Table 4). The Na, K, and Al concentrations were also analyzed by FE-EPMA and their concentrations in the product glasses are similar within error to the starting glass compositions given in Table 2.

In the fluid-melt interaction experiments for the Ta-bearing system, no Ta phase crystallized at 700 °C, which is a consequence of tantalite-(Mn) being too soluble in peralkaline melts of low ASI_{Li} (approximately 0.90). At 650 °C, nanometer-sized calcium (Ca)-Ta oxide crystallized (Figure 2), which is very likely microlite based on FE-EPMA-EDS analyses, but the solubility product cannot be calculated (McNeil 2018). As Ca was not added to any experiment, additional experiments are needed to determine saturation values for tantalite-(Mn) and

362 microlite. However, it is noteworthy that microlite is commonly interpreted to be metasomatic in
363 natural systems (London et al. 1988).
364
365 **Textures observed**
366 Despite crystallization from fluid-melt interactions (from the interaction of a Mn-rich
367 fluid with a Nb- or Ta-rich melt), the textures observed in the experimental run products are
368 strictly magmatic (phenocrysts in a glass matrix). In higher temperature experiments that did not
369 crystallize anorthoclase (700 °C, Figure 3), both columbite-(Mn) and lithiophilite are observed as
370 individual, euhedral crystals that are randomly oriented and show no zoning or alteration. Both
371 of these minerals formed from fluid-melt interactions, as the Mn necessary to crystallize
372 lithiophilite and columbite-(Mn) came from the fluid and not the melt. In lower temperature
373 experiments (Nb at 650 °C, Figure 1 and Ta at 650 °C, Figure 2) anorthoclase crystallized in
374 addition to lithiophilite in both experiments, and columbite-(Mn) in the Nb-doped glass
375 experiment, and a Ta-Ca oxide (likely microlite) in the Ta-doped glass experiment. Both 650 °C
376 and 700 °C experiments exhibit purely magmatic textures. It can be deduced that the columbite-
377 (Mn), Ca-Ta oxide, and lithiophilite formed first in their respective experiments, as they are
378 found as inclusions within the anorthoclase. However, they are also interstitial and therefore are
379 also syn- or post-anorthoclase crystallization. We assume that the anorthoclase
380 ($Na_{0.62}K_{0.36}Al_{1.04}Si_{2.97}O_8$) formed from the melt as all elements required for crystallization are
381 present in the melt. However, the hydrothermal fluid also contained Na and K in similar
382 proportions to the melt composition, and we cannot rule out that the fluid played a role in the
383 crystallization of the anorthoclase. Similarly, it is not possible to determine the origin of the Ca-
384 Ta oxide (assumed to be microlite). Both the melt and the fluid contained only trace impurities of

385 Ca (< 170 ppm glass and < 22 ppm fluid). Therefore, the fluid could have played a role in the
386 crystallization of the Ca-Ta oxide, but the source of the Ta was the melt.
387
388 **Columbite-(Mn) solubility**
389 The solubility products for columbite-(Mn) and lithiophilite (molar $LiO_{0.5}{\cdot}MnO{\cdot}PO_{2.5}$
390 product) are reported in Table 4. The solubility of columbite-(Mn) is highly temperature
391 dependent (Figure 4), in agreement with previous research (e.g. Linnen and Keppler 1997;
392 Chevychelov et al. 2010; Aseri et al. 2015; McNeil 2018). The $\log K_{sp}$ values of columbite-(Mn)
393 for the dissolution experiments are identical within error to those of the crystallization (reverse)
394 and repeat dissolution experiments at the same temperature, thus it can be concluded that the
395 solubility products from these experiments are equilibrium values. Furthermore, the fluid-melt
396 interaction experiments have an identical solubility product within error (-2.92 $mol^2/kg^2 \pm 0.02$)
397 to the dissolution (-2.90 $mol^2/kg^2 \pm 0.02$) and crystallization (reversal) (-2.89 $mol^2/kg^2 \pm 0.01$)
398 experiments at the same temperature (700 °C), demonstrating that experiments performed
399 utilizing this method also attain equilibrium. This is significant because the crystallization
400 mechanisms in the two sets of experiments are very different (fluid-melt interactions versus
401 purely magmatic). This demonstrates that our solubility products represent equilibrium values
402 and are independent of how saturation was attained. Note that the concentrations of Nb and Mn
403 are different in different experiments. Since the solubility product is constant for the range of Nb
404 and Mn concentrations, Henrian behavior is demonstrated (i.e. the activity coefficients are
405 constant for the range of compositions examined; Wood and Fraser, 1977). Although
406 experiments on granitic melts have examined silicate phase equilibria at lower temperatures, it is
407 not possible to determine the solubilities of many accessory phases at these temperatures due to

the slow diffusivities of HFSEs (Mungall et al. 1999). The previous reported lowest temperature solubility experiment was at 650 °C (Chevychelov et al. 2010), with experiments most commonly completed at 800 °C or higher. These fluid-melt interaction experiments are revolutionary as they do not require HFSE diffusion in melts to attain equilibrium, only the fluid mobile elements are required to diffuse across the distance of the glass grain size (typically <100 microns) as the fluid surrounds the grains. This diffusion can occur rapidly and allows for experiments to be conducted at lower temperatures, in the range that flux-rich granitic melts crystallize. This is extremely important for experiments on Sn minerals such as wodginite, as Sn alloys with gold experiment capsules at temperatures greater than 700 °C (e.g. McNeil 2018).

The enthalpy of dissolution or formation can be calculated via the integrated Van't Hoff equation (Wood and Fraser 1977) and are reported in Table 6. If melts at constant pressure and bulk composition exhibit the same temperature dependence, but have variable Mn-Nb-Ta contents, then Henrian behavior is demonstrated (Linnen and Keppler 1997) and enthalpies of formation can be used to demonstrate equilibrium. The enthalpy of formation of columbite-(Mn) from fluid-melt interaction experiments is identical within error to the enthalpy of dissolution from dissolution experiments, indicating that the solubility products from the fluid-melt interaction experiments are equilibrium values. However, it is difficult to compare the enthalpies determined here to those of other studies because the melt compositions and thus enthalpies of those studies are different.

Lithiophilite solubility

To the knowledge of the authors, lithiophilite solubility products reported for haplogranitic melt compositions (Table 4) and the enthalpy of formation of lithiophilite (Table 6) have not previously been reported. Lithiophilite also involves FMEs (Li-Mn) and a HFSE

(phosphorus, P) and its solubility displays a strong temperature dependence, similar to other HFSE-bearing minerals.

Experiments that contain lithiophilite will remove lithium from the melt because lithiophilite contains approximately 12% Li_2O. Anorthoclase crystallization will concentrate lithium in the melt because lithium is an incompatible element in feldspars with experimental partition coefficients determined for plagioclase between An_{80} and An_{40} of $K_{Li}^{Pl/melt} = 0.25 \pm 0.04$ (Bindeman et al. 1998, Bindeman and Davis 2000). Additionally, Li has been shown to partition into the fluid (vapor) from a melt (London et al. 1988), therefore some lithium was likely exchanged with the fluid phase during the experiments. Assuming the difference in phosphorus concentration between the starting glass and experiment represents the amount of lithiophilite that crystallized due to low fluid-melt partition coefficients for phosphorus (London et al. 1988, Keppler 1994), the amount of lithium that would have been removed due to lithiophilite crystallization in the Nb glass 650 °C experiment (SMn1Nb5000-650) is 0.10 wt% Li_2O. The actual difference in concentration between the starting glass and final experiment is 0.34 wt% Li_2O. Therefore, lithium must have also been removed from the melt and exchanged for cations in the fluid phase.

Discussion

The solubility product of columbite-(Mn) is predicted to be -4.75 mol^2/kg^2, by extrapolating the linear regression to 450 °C (Figure 4), which can be used to calculate predicted Nb and Ta melt concentrations at this temperature and pressure. If a melt contains stoichiometric proportions of Nb and Mn this corresponds to approximately 1100 ppm Nb and 300 ppm Mn. This Nb concentration is much higher than reported values from natural pegmatites (8 to 238 ppm, Borisova et al. 2012; Webster et al. 1997; Zajacz et al. 2008). Alternatively, this study has

454 shown that columbite-(Mn) can crystallize as a result of Mn fluid interaction with a HFSE
455 enriched melt at the magmatic stage. For fluid-melt interaction crystallization from a flux-rich
456 pegmatite melt at 450 °C, our data shows that only 17 ppm Nb is needed to reach saturation in
457 columbite-(Mn) where 1 wt% Mn is present in a coexisting fluid. This is a reasonable
458 concentration based on natural reported Nb concentrations at pegmatites such as
459 Ehrenfriedersdorf (Zajacz et al. 2008) or Tanco (Stilling et al. 2006).

460 As water is incompatible (and CO_2 and other volatiles), the crystallization of a silicate
461 melt will eventually lead to fluid saturation. Our experiments demonstrate that for melts at fluid-
462 saturated conditions it is possible that mobile cations (FME) may play an important role in
463 mineralization. For flux- and rare metal-rich haplogranitic melts with hundreds of ppm Nb or Ta,
464 columbite-(Mn) or tantalite-(Mn) can crystallize from interaction with a Mn-rich hydrothermal
465 fluid (with either an external source or derived internally from a different part of the granite or
466 pegmatite). As CGM mineralization typically occurs disseminated in the apical parts of rare
467 metal granites and throughout pegmatite bodies, the fluid may have been internally derived,
468 which is consistent with work on natural examples (e.g. Borisova et al. 2012). There will be a
469 competition for Mn between oxide, silicate and phosphate minerals. Solubility products from this
470 study show that lithiophilite can crystallize before columbite-(Mn). However, changing the
471 concentrations of Li and P in the melt could change this order, and the stability of different
472 phosphate species is an additional complexity. Given that columbite-(Mn), lithiophilite and
473 potentially a Ca-Ta oxide mineral successfully crystallized from fluid-melt interactions, it is
474 likely that other Nb, Ta, and Li minerals (e.g. pyrochlore, tantalite-(Mn or Fe), columbite-(Fe),
475 wodginite, triphylite, amblygonite or lepidolite) will also crystallize from Na-, K-, Ca-, Fe-, Mn-,
476 or Sn-rich fluids. It is interesting to note that a recent experimental study replicated columbite

group mineral textures by supersaturation (Van Lichtervelde et al. 2018). Supersaturation in those experiments was produced by strong undercooling, but the current study raises the possibility that supersaturation could also result from the introduction of FMEs to the melt via fluids.

Implications

The experiments described above establish an experimental technique to investigate solubilities of minerals in melts through the interaction of a HFSE-rich melt with a FME-rich fluid. These experiments demonstrate an alternative approach to reaching equilibrium and allow for experiments to be completed more confidently at lower temperatures without the issue of slow diffusion of HFSEs. These experiments were completed to 650 °C, but with the correct glass composition (to allow for the melt to remain a glass for as long as possible) experiments can be completed to even lower temperatures. This opens the possibility for future experiments on minerals that contain elements such as Sn, that alloy with gold experiment capsules at temperatures above 700 °C. This experimental method can also be used to reverse dissolution solubility experiments and to evaluate Henry's Law behaviour of solubility products.

Magmatic chloride-bearing fluids complex metals such as Fe, Mn and Sn (Webster and Holloway 1988). Our experiments showed that moderately saline fluids could provide the necessary concentration of Mn to a local melt and result in the crystallization of columbite-(Mn) and lithiophilite. The textures observed in this study are consistent with a wholly magmatic origin. However, we know that crystallization was triggered by fluid-melt interactions. This has significant implications for rare-metal deposits as the majority of interpretations as to whether magmatic or fluid-melt processes occur is based on textural evidence, when this study has now shown that textures from fluid-melt interactions may not be observed. This has implications to

natural systems, as textures and mineralization previously considered to be strictly magmatic may have had influence from a fluid on rare metal mineralization that, due to low Nb or Ta concentrations (well below saturation values), was not previously well explained. The reverse may also be true; that textures previously interpreted to be purely from fluid-melt interactions (e.g. hydrothermal or metasomatic) may in part be magmatic or have a magmatic influence. This is significant as many Nb and Ta deposits worldwide exhibit textural evidence of hydrothermal or metasomatic events, which in the literature have been termed greisenization (e.g., at Tanco, Černý (2005); or Manono-Kitotolo, Katanga, Democratic Republic of Congo, Dewaele et al. 2016) or secondary saccharoidal albite at the Brazil Lake pegmatite, Nova Scotia, Canada (Kontak 2006). Other rare metal granites and pegmatites that have evidence of metasomatism include Varuträsk, Northern Sweden (Siegel et al. 2016), Cínovec/Zinnwald, Czech Republic (Breiter et al. 2017), Dajishan, Southeastern China (Wu et al. 2017), and Yichun, Southeastern China (Wu et al. 2018). Additionally, metasomatism has previously been proposed to explain the crystallization of tourmaline at Tanco, with Mg and Ti having been derived from the host amphibolite (Selway et al., 2000). Similarly, the classic model for some pegmatite-hosted emerald deposits is that the granitic melt provides the Be for beryl and the Cr and V (chromophores for the green color of emerald) are the result of metasomatism of an ultramafic or mafic wallrock (Groat et al. 2014).

Lastly, it is interesting to point out that during these experiments, lithium mineralization (lithiophilite crystallization) occurred from diffusion of Mn into the melt. This crystallization occurred in spite of the loss of Li to the fluid from the melt in the experiments. Lithium haloes around LCT pegmatites are typically used as exploration tools as they radiate outwards from the pegmatite (Trueman and Černý, 1982). Lithium that was partitioned into the fluids that emanate

from LCT pegmatites can potentially exchange FMEs (e.g. Mn, Fe) from hydrothermal fluids from the host rock, and these fluids could play a role in the crystallization of Nb/Ta minerals such as CGMs, wodginite and pyrochlore supergroup minerals.

Acknowledgements

The authors would like to gratefully acknowledge NSERC Discovery Grants to R.L. Linnen and R.L. Flemming for funding this research. We would also like to acknowledge an Ontario Government Queen Elizabeth II Graduate Scholarship in Science and Technology to A.G. McNeil in support of this research, as well as a Mineralogical Association of Canada Student Travel Grant awarded for presentation of this research at RFG 2018 in Vancouver, British Columbia, Canada. Our thanks are extended to M. Beauchamp for help with microprobe analyses, A. Aseri for his advice and guidance with respect to experiments, M.J. Walzak at Surface Science Western for Raman analyses, and R. Sharpe at the University of Manitoba for assistance with SIMS analyses.

References cited

Anderson, S.D. (1992) Mineralogy, geochemistry and structure of a tantalum-bearing pegmatite swarm, Bernic lake, Manitoba. Ph.D. dissertation. University of Manitoba, Canada.

Aseri, A.A., Linnen, R.L., Che, X.D., Thibault, Y., and Holtz, F. (2015) Effects of fluorine on the solubilities of Nb, Ta, Zr, and Hf minerals in highly fluxed water-saturated haplogranitic melts. Ore Geology Reviews, 64, 736-746.

Bartels, A., Holtz, F., and Linnen, R.L. (2010) Solubility of manganotantalite and manganocolumbite in pegmatitic melts. American Mineralogist, 95, 537-544.

545 Bindeman, I.N., and Davis, A.M. (2000) Trace element partitioning between plagioclase and
546 melt: investigation of dopant influence on partition behavior. Geochimica et
547 Cosmochimica Acta, 64, 2863-2878.
548 Bindeman, I.N., Davis, A.M., and Drake, M.J. (1998) Ion microprobe study of plagioclase basalt
549 partition experiments at natural concentration levels of trace elements. Geochimica et
550 Cosmochimica Acta, 62, 1175-1193.
551 Borisova, A.Y., Thomas, R., Salvi, S., Candaudap, F., Lanzanova, A., and Chmeleff, J. (2012)
552 Tin and associated metal and metalloid geochemistry by femtosecond LA-ICP-QMS
553 microanalysis of pegmatite–leucogranite melt and fluid inclusions: new evidence for
554 melt–melt–fluid immiscibility. Mineralogical Magazine, 76, 91-113.
555 Borodulin, G.P., Chevychelov, V.Yu., and Zaraysky, G.P. (2009) Experimental study of
556 partitioning of tantalum, niobium, manganese, and fluorine between aqueous fluoride
557 fluid and granitic and alkaline melts. Doklady Earth Sciences, 427, 868-873.
558 Breiter, K., Korbelová, Z., Chládek, S., Uher, P., Knesl, I., Rambousek, P., Honig, S., and
559 Šešulka, V. (2017) Diversity of Ti–Sn–W–Nb–Ta oxide minerals in the classic granite-
560 related magmatic–hydrothermal Cínovec/Zinnwald Sn–W–Li deposit (Czech Republic).
561 European Journal of Mineralogy, 29, 727-738.

562 Burdo, R.A., and Morrison, G.H. (1971) Table of atomic and molecular lines for spark source
563 mass spectrometry of complex sample-graphite mixes: Materials Science Center Report
564 #1670, Cornell University, Ithaca, New York.
565 Černý, P. (1986) Characteristics of pegmatite deposits of tantalum. Lanthanides, tantalum and
566 niobium, 195-239.

Černý, P. (2005) The Tanco rare-element pegmatite deposit, Manitoba: Regional context, internal anatomy, and global comparisons. In Linnen, R.L. and Samson, I.M., Eds., Rare-Element Geochemistry and Mineral Deposits, p.127-152. Geological Association of Canada, GAC Short Course Notes 17.

Černý, P. and Ercit, T.S. (2005) The classification of granitic pegmatites revisited. The Canadian Mineralogist, 43, 2005-2026.

Cheng, L., Zhang, C., Yang, X., Qi, D., Zhou, Y., and Holtz, F. (2019) Experimental investigation of reactions between two-mica granite and boron-rich fluids: Implications for the formation of tourmaline granite. Science China Earth Sciences, 62, 1630-1644.

Chevychelov, V.Y., Borodulin, G.P., and Zaraisky, G.P. (2010) Solubility of columbite, (Mn, Fe)(Nb, Ta)$_2$O$_6$, in granitoid and alkaline melts at 650-850°C and 30-400MPa: An experimental investigation. Geochemistry International, 48, 456-464.

Choi, M.S., Ryu, J-S., Park, H.Y., Lee, K-S., Kil, Y., and Shin, H.S. (2013) Precise determination of the lithium isotope ratio in geological samples using MC-ICP-MS with cool plasma. Journal of Analytical Atomic Spectrometry, 28, 505-509.

Cuney, M., Marignac, C., and Weisbrod, A. (1992) The Beauvoir topaz-lepidolite albite granite (Massif Central, France): The disseminated magmatic Sn-Li-Ta-Nb-Be mineralization. Economic Geology, 87, 1766-1794.

Dewaele, S., Hulsbosch, N, Cryns, Y., Boyce, A., Burgess, R., and Muchez, Ph. (2016) Geological setting and timing of the world-class Sn, Nb–Ta and Li mineralization of Manono-Kitotolo (Katanga, Democratic Republic of Congo). Ore Geology Reviews, 72, 373-390.

589 Elliot, H.A.L., Wall, F., Chakhmouradian, A.R., Siegfried, P.R., Dahlgren, S., Weatherley, S.,
590 Finch, A.A., Marks, M.A.W., Dowman, E., and Deady, E. (2018) Fenites associated with
591 carbonatite complexes: A review. Ore Geology Reviews, 93, 38–59.
592 Fetherston, J.M. (2004) Tantalum in Western Australia. Geological Survey of Western Australia
593 Mineral Resources Bulletin 22, 162 p.
594 Fiege, A., Kirchner, C., Holtz, F., Linnen, R.L., and Dziony, W. (2011) Influence of fluorine on
595 the solubility of manganotantalite ($MnTa_2O_6$) and manganocolumbite ($MnNb_2O_6$) in
596 granitic melts — An experimental study. Lithos, 122, 165-174.
597 Fiege, A., Simon, A., Linsler, S.A., Bartels, A., and Linnen, R.L. (2018) Experimental
598 constraints on the effect of phosphorous and boron on Nb and Ta ore formation. Ore
599 Geology Reviews, 94, 383-395.
600 Flemming, R.L. (2007) Micro X-ray diffraction (μXRD): a versatile technique for
601 characterization of Earth and planetary materials. Canadian Journal of Earth Sciences, 44,
602 1333-1346.
603 Frank, M.R., Candela, P.A., and Piccoli, P.M. (2003) Alkali exchange equilibria between a
604 silicate melt and coexisting magmatic volatile phase: An experimental study at 800°C and
605 100 MPa. Geochimica et Cosmochimica Acta, 67, 1415-1427.
606 Graedel, T.E., Harper, E.M., Nassar, N.T., Nuss, P. and Reck, B.K. (2015) Criticality of metals
607 and metalloids. Proceedings of the National Academy of Sciences, 112, 4257-4262.

608 Groat, L.A., Giuliani, G., Marshall, D., and Turner, D.J. (2014) Emerald. In Groat, L.A. Ed.,
609 Geology of Gem Deposits, p135-174. Mineralogical Association of Canada 44.
610 Holtz, F., Dingwell, D.B., and Behrens, H. (1993) Effects of F, B_2O_3 and P_2O_5 on the solubility
611 of water in haplogranite melts compared to natural silicate melts. Contributions to
612 Mineralogy and Petrology, 113, 492-501.
613 Keppler, H. (1993) Influence of fluorine on the enrichment of high field strength trace elements
614 in granitic rocks. Contributions to Mineralogy and Petrology, 114, 479-488.
615 Keppler, H. (1994) Partitioning of phosphorus between melt and fluid in the system
616 haplogranite-H_2O-P_2O_5. Chemical Geology, 117, 345-353.
617 Kjarsgaard, B.A., and Mitchell, R.H. (2008) Solubility of Ta in the system $CaCO_3$ – $Ca(OH)_2$ –
618 $NaTaO_3$ – $NaNbO_3$ ± F at 0.1 GPa: Implications for the crystallization of pyrochlore-
619 group minerals in carbonatites. The Canadian Mineralogist, 46, 981-990.
620 Kontak, D.J. (2006) Nature and origin of an LCT-suite pegmatite with late-stage sodium
621 enrichment, Brazil Lake, Yarmouth County, Nova Scotia. I. Geological setting and
622 petrology. The Canadian Mineralogist, 44, 563-598.
623 Linnen, R.L. (1998) The Solubility of Nb-Ta-Zr-Hf-W in granitic melts with Li and Li + F:
624 Constraints for mineralization in rare metal granites and pegmatites. Economic Geology,
625 93, 1013-1025.
626 Linnen, R.L., and Keppler, H. (1997) Columbite solubility in granitic melts: consequences for
627 the enrichment and fractionation of Nb and Ta in the Earth's crust. Contributions to
628 Mineralogy and Petrology, 128, 213-227.
629 Linnen, R.L., Samson, I.M., Williams-Jones, A.E., and Chakhmouradian, A.R. (2014)
630 Geochemistry of the Rare-Earth Element, Nb, Ta, Hf, and Zr Deposits. In Holland, H.D.,

631 and Turekian, K.K. Eds., Treatise on Geochemistry (2nd Edition), Pages 534-568.
632 Elsevier. https://doi.org/10.1016/B978-0-08-095975-7.01124-4.
633 Linnen, R.L., Trueman, D.L. and Burt, R. (2014) Niobium and Tantalum. In G. Gunn, Ed.,
634 Critical Metals Handbook, p. 361-384, John Wiley & Sons.
635 London, D. (2008) Pegmatites. The Canadian Mineralogist Special Publication 10, 347 p.
636 London, D. (2018) Ore-forming processes within granitic pegmatites. Ore Geology Reviews,
637 101, 349-383.
638 London, D., Hervig, R.L., and Morgan, G.B. VI. (1988) Melt-vapor solubilities and elemental
639 partitioning in peraluminous granite-pegmatite systems: experimental results with
640 Macusani glass at 200 MPa. Contributions to Mineralogy and Petrology, 99, 360-373.
641 Mackay, D.A.R. and Simandl, G.J (2014) Geology, market and supply chain of niobium
642 and tantalum—a review. Mineralium Deposita, 49, 1025–1047.

643 Maner, J.L. IV., London. D., and Icenhower, J.P. (2019) Enrichment of manganese to spessartine
644 saturation in granite-pegmatite systems. American Mineralogist, 104, 1625-1637.

645 Marks, M.A.W., and Markl, G. (2017) A global review on agpaitic rocks. Earth-Science
646 Reviews, 173, 229–258.

647 Matthews, W., Linnen, R.L., and Guo, Q. (2003) A filler-rod technique for controlling redox
648 conditions in cold-seal pressure vessels. American Mineralogist, 88, 701-707.

649 McNeil, A.G. (2018) Crystallization processes and solubility of columbite-(Mn), tantalite-(Mn),
650 microlite, pyrochlore, wodginite and titanowodginite in highly fluxed haplogranitic melts,
651 415p. Ph.D. thesis Western University, London, Ontario, Electronic Thesis and
652 Dissertation Repository 5261.

McNeil, A.G., Linnen, R.L., and Flemming, R.L. (2015) Hydrothermal synthesis of columbite-(Mn), tantalite-(Mn), hafnon, and zircon at 800-850 °C and 200 MPa. The Canadian Mineralogist, 53, 1073-1081.

McNeil, A.G., Linnen, R.L., and Flemming R.L. (2019) Solubility of wodginite, titanowodginite, microlite, pyrochlore, columbite-(Mn) and tantalite-(Mn) in flux-rich haplogranitic melts between 700°-850 °C and 200 MPa. Lithos, in press DOI: 10.1016/j.lithos.2019.105239.

Morgan, G.B. VI and London, D. (1996) Optimizing the electron microprobe analysis of hydrous alkali aluminosilicate glasses. American Mineralogist, 81, 1176-1185.

Müller, A., Spratt, J., Thomas, R., Williamson, B.J., and Seltmann, R. (2018) Alkali-F-rich albite zones in evolved NYF pegmatites: the product of melt-melt immiscibility. The Canadian Mineralogist, 56, 657-687.

Mungall, J.E., Dingwell, D.B., and Chaussidon, M. (1999) Chemical diffusivities of 18 trace elements in granitoid melts. Geochimica et Cosmochimica Acta, 63, 2599-2610.

Partington, G.A., McNaughton, N.J., and Williams, I.S. (1995) A review of the geology, mineralization, and geochronology of the Greenbushes Pegmatite, Western Australia. Economic Geology, 90, 616-635.

Patino-Douce, M. L., Patino-Douce, A., Qayyum, M. and Nielsen, R. L. (1994) New set of low concentration standards for La, Ce, Sm, Yb, Lu, Y, Sc, V, Nb and Ta in silicates. Geostandards Newsletter, 18, 195-198.

Pearce, M.J.G, Perkins, W.T., Westgate, J.A., Gorton, M.P., Jackson, S.E., Neal, C.R., and Chenery, S.P. (1997) A compilation of new and published major and trace element data for NIST SRM 610 and NIST SRM 612 glass reference materials. Geostandards Newsletter, 21, 115-144.

676 Qi, H.P., Coplen, T.B., Wang, Q.Zh., and Wang, Y.H. (1997) Unnatural isotopic composition of
677 lithium reagents. Analytical Chemistry, 69, 4076-4078.
678 Raimbault, L., Cuney, M., Azencott, C., Duthou, J.L., and Joron, J.L. (1995) Geochemical
679 evidence for a multistage magmatic genesis of Ta-Sn-Li mineralization in the granite at
680 Beauvoir, French Massif Central. Economic Geology, 90, 548-576.
681 Rao, C., Wang, R.C., Hu, H., and Zhang, W.L. (2009) Complex internal textures in oxide
682 minerals from the Nanping No. 31 dyke of granitic pegmatite, Fujian Province,
683 Southeastern China. The Canadian Mineralogist, 47, 1195-1212.
684 Schulz, K., and Papp, J. (2014) Niobium and Tantalum—Indispensable Twins. USGS Fact Sheet
685 3054**.**
686 Schwartz, M.O. (1992) Geochemical criteria for distinguishing magmatic and metasomatic
687 albite-enrichment in granitoids - examples from the Ta-Li granite Yichun (China) and the
688 Sn-W deposit Tikus (Indonesia). Mineralium Deposita, 27, 101-108.
689 Selway, J.B., Černý, P., and Hawthorne, F.C. (2000) The Tanco pegmatite and Bernic Lake,
690 Manitoba. XIV. Internal tourmaline. The Canadian Mineralogist, 38, 877-891.
691 Siegel, K., Wagner, T., Trumbull, R.B., Jonssond, E., Matalin, G., Wälle, M., and Heinrich, C.A.
692 (2016) Stable isotope (B, H, O) and mineral-chemistry constraints on the magmatic to
693 hydrothermal evolution of the Varuträsk rare-element pegmatite (Northern Sweden).
694 Chemical Geology, 421, 1-16.
695 Sowerby, J.R. and Keppler, H. (2002) The effect of fluorine, boron and excess sodium
696 on the critical curve in the albite–H_2O system. Contributions to Mineralogy and
697 Petrology, 143, 32-37.

698 Stilling, A., Černý, P., and Vanstone, P.J. (2006) The Tanco pegmatite at Bernic Lake, Manitoba.
699 XVI. Zonal and bulk compositions and their petrogenetic significance. The Canadian
700 Mineralogist, 44, 599-623.
701 Tang, Y., and Zhang, H. (2015) An experimental determination of W, Nb, and Ta partition
702 coefficients between P-rich peraluminous granitic melt and coexisting aqueous fluid.
703 Chinese Journal of Geochemistry, 34, 194-200.
704 Tang, Y., Zhang, H., and Rao, B. (2016) The effect of phosphorus on manganocolumbite and
705 manganotantalite solubility in peralkaline to peraluminous granitic melts. American
706 Mineralogist, 101, 415-422.
707 Timofeev, A., Migdisov, Art. A., and Williams-Jones, A.E. (2015) An experimental study of the
708 solubility and speciation of niobium in fluoride-bearing aqueous solutions at elevated
709 temperature. Geochimica et. Cosmochimica Acta, 158, 103-111.
710 Timofeev, A., Migdisov, Art. A., and Williams-Jones, A.E. (2017) An experimental study of the
711 solubility and speciation of tantalum in fluoride-bearing aqueous solutions at elevated
712 temperature. Geochimica et. Cosmochimica Acta, 197, 294-304.
713 Thomas, R., and Davidson, P. (2016) Revisiting complete miscibility between silicate melts and
714 hydrous fluids, and the extreme enrichment of some elements in the supercritical state —
715 Consequences for the formation of pegmatites and ore deposits. Ore Geology Reviews,
716 72, 1088-1101.
717 Thomas, R., Davidson, P., and Beurlen, H. (2011) Tantalite-(Mn) from the Borborema Pegmatite
718 Province, northeastern Brazil: conditions of formation and melt and fluid-inclusion
719 constraints on experimental studies. Mineralium Deposita, 46, 749–759.

720 Trueman, D.L. and Černý, P. 1982, Exploration for rare-element granitic pegmatites. In P. Černý
721 Ed., Granitic Pegmatites in Science and Industry. Mineralogical Association of Canada
722 Short Course 8, 463-493.
723 Van Lichtervelde, M., Linnen, R.L., Salvi, S. and Didier, B. (2006) The role of metagabbro rafts
724 on tantalum mineralization in the Tanco granitic pegmatite, Manitoba. The Canadian
725 Mineralogist, 44, 625-644.
726 Van Lichtervelde, M., Linnen, R.L., Salvi, S. and Didier, B. (2007) Textures and chemical
727 evolutions in tantalum oxides: a discussion of magmatic versus metasomatic origins for
728 Ta mineralization in the Tanco Lower Pegmatite, Manitoba, Canada. Economic Geology,
729 102, 257-276.
730 Van Lichtervelde, M., Holtz, F., and Hanchar, J.M. (2010) Solubility of manganotantalite, zircon
731 and hafnon in highly fluxed peralkaline to peraluminous pegmatitic melts. Contributions
732 to Mineralogy and Petrology, 160, 17-32.
733 Van Lichtervelde, M., Holtz, F., and Melcher, F. (2018) The effect of disequilibrium
734 crystallization on Nb-Ta fractionation in pegmatites: Constraints from crystallization
735 experiments of tantalite-tapiolite. American Mineralogist, 103, 1401-1416.
736 Webster J.D., and Holloway J.R. (1988) Experimental constraints on the partitioning of C1
737 between topaz rhyolite melt and H_2O and $H_2O + CO_2$ fluids; new implications for granitic
738 differentiation and ore deposition. Geochimica et Cosmochimica Acta, 52, 2091-2105.
739 Webster, J.D., Thomas, R., Rhede, D., Förster, H-J., and Seltmann, R. (1997) Melt inclusions in
740 quartz from an evolved peraluminous pegmatite: Geochemical evidence for strong tin
741 enrichment in fluorine-rich and phosphorus-rich residual liquids. Geochimica et
742 Cosmochimica Acta, 61, 2589-2604.

743 Wood, B.J., and Fraser, D.G. (1977) Elementary Thermodynamics for Geologists, 303 p. Oxford
744 University Press.
745 Wu, M., Samson, I.M., and Zhang, D. (2017) Textural and chemical constraints on the formation
746 of disseminated granite-hosted W-Ta-Nb mineralization at the Dajishan deposit, Nanling
747 Range, Southeastern China. Economic Geology, 112, 855–887.
748 Wu, M., Samson, I.M., and Zhang, D. (2018) Textural features and chemical evolution in Ta-Nb
749 oxides: Implications for deuteric rare-metal mineralization in the Yichun Granite-
750 Marginal Pegmatite, Southeastern China. Economic Geology, 113, 937-960.

751 Yin, L., Pollard, P.J., Shouxi, H., and Taylor, R.G. (1995) Geological and Geochemical
752 Characteristics of the Yichun Ta-Nb-Li Deposit, Jiangxi Province, South China.
753 Economic Geology, 90, 577-585.
754 Zajacz, Z., Halter, W.E., Pettke, T., and Guillong, M. (2008) Determination of fluid/melt
755 partition coefficients by LA-ICPMS analysis of co-existing fluid and silicate melt
756 inclusions: Controls on element partitioning. Geochimica et Cosmochimica Acta, 72,
757 2169-2197.
758 Zaraisky, G.P., Korzhinskaya, V. and Kotova, N. (2010), Experimental studies of Ta_2O_5 and
759 columbite-tantalite solubility in fluoride solutions from 300 to 550°C and 50 to 100 MPa.
760 Mineralogy and Petrology 99, 287-300.
761
762
763
764
765

This is a preprint, the final version is subject to change, of the American Mineralogist (MSA)
Cite as Authors (Year) Title. American Mineralogist, in press.
DOI: https://doi.org/10.2138/am-2020-7216

766

Tables

Table 1. Summary of typical characteristics of deposit types that host Nb-Ta mineralization

Characteristics	LCT pegmatites and Rare-metal granites[1,2,3,4,5,6]	Rare-metal carbonatites[1,2,7,8]	Alkaline complexes[2,7,9]
General lithology (varies greatly between deposits)	**Pegmatite:** Granitic pegmatite ± muscovite, tourmaline, HFSE minerals such as CGMs, wodginite, and microlite, Li silicates, pollucite, beryl; **Rare-metal granite:** Granite ± HFSE minerals such as CGMs, wodginite and microlite, Li silicates, lepidolite, cassiterite, topaz	Carbonatite (50% or more of modal carbonate) + HFSE minerals such as CGMs and pyrochlore group minerals	Peralkaline igneous ± HFSE minerals such as eudialyte, zircon, pyrochlore group minerals
Concentrate Nb or Ta (minerals associated)	Ta and Nb (economic in columbite-tantalite, with accessory wodginite and microlite)	Nb and Ta (economic in pyrochlore and columbite)	Nb and Ta (economic in pyrochlore and columbite)
ASI of melt	Metaluminous to Peraluminous (ASI 1.0 and greater)	n/a*	Peralkaline (ASI < 1)
Potentially associated fluid	Typically aqueous near neutral pH and Cl/F-rich	highly variable aqueous to CO2-rich or high pH, alkali-rich (fenite alteration)	highly variable aqueous to CO2-rich or high pH, alkali-rich (fenite alteration)
Solubility of Nb/Ta in fluid	negligible	Nb in fenites	Nb in fenites
Solubility of Nb/Ta minerals in melt	very high (up to wt% levels) at temperatures greater than 700 °C	very high (up to wt% levels) at temperatures greater than 700 °C	very high (up to wt% levels) at temperatures greater than 700 °C

*n/a = not applicible because ASI is a compositional classification of granitic melts, however carbonatites are associated with alkaline rocks

[1]Linnen, Samson et al. (2014), [2]Mackay and Simandl (2014), [3]Černý and Ercit (2005), [4]Raimbault et al. (1995), [5]Borodulin et al. (2009), [6]Zajacz et al. (2008), [7]Elliot et al. (2018), [8]Kjarsgaard and Mitchell (2008), [9]Marks and Markl (2017)

767

768

769

770

771 Table 2. Starting glass compositions.

Oxides	PEGA (wt%)	NBD-5000ppm (wt%)	TAD-5000ppm (wt%)	PEGA-H1 (wt%)
SiO_2	63.75 (±1.08)*	59.96 (±0.63)*	60.47 (±0.96)*	59.31 (±1.05)*
Al_2O_3	17.85 (±0.49)*	16.72 (±0.48)*	16.63(±0.45)*	16.39 (±0.62)*
K_2O	4.39 (±0.18)*	4.08 (±0.12)*	4.07 (±0.10)*	4.05 (±0.19)*
Na_2O	8.34 (±0.44)*	7.31 (±0.39)*	7.30 (±0.43)*	7.26 (±0.50)*
P_2O_5	1.66 (±0.19)*	1.56 (±0.21)*	1.56 (±0.26)*	1.53 (±0.13)*
Nb_2O_5	-	0.73 (±0.18)*	-	-
Ta_2O_5	-	-	0.67 (±0.07)*	-
F	0.76 (±0.44)*	0.91 (±0.27)*	0.92 (±0.28)*	0.93 (±0.27)*
B_2O_3	2.36 (±0.06)#	2.36 (±0.06)#	2.36 (±0.06)#	2.36 (±0.06)#
Li_2O	1.05 (±0.04)#	1.05 (±0.04)#	1.05 (±0.04)#	1.05 (±0.04)#
2F=O	-0.32	-0.38	-0.39	-0.39
Total	99.84	94.30	94.64	92.49
H_2O (by difference)	-	5.70	5.36	7.51
ASI**	0.97	1.02	1.01	1.00
ASI_{Li}##	0.81	0.83	0.83	0.82

Notes:

3σ standard deviation is given in parentheses

PEGA is the anhydrous base glass for all starting materials

PEGA-H1 is the hydrous PEGA glass for dissolution, crystallization and repeat experiments

NBD & TAD are Nb and Ta doped glasses, respectively, for fluid-melt interaction experiments

* Measured by EPMA

Measured by Actlabs ICP-MS from initial PEGA glass

** ASI molar ratio of Al/(Na+K)

ASI_{Li} molar ratio of Al/(Na+K+Li)

772

773 Table 3. Starting fluid composition. Errors reported are 1σ standard deviation of three analyses.

Compound	1% Mn fluid (wt%)
Mn (as $MnCl_2$)	1.01 ±0.08 (2.32 ±0.17)
NaCl	3.60 (±0.25)
KCl	2.19 (±0.18)
H_2O (calculated by difference)	91.89

774

This is a preprint, the final version is subject to change, of the American Mineralogist (MSA)
Cite as Authors (Year) Title. American Mineralogist, in press.
DOI: https://doi.org/10.2138/am-2020-7216

Table 4. Experiment details, EPMA glass analyses, columbite-(Mn) and lithiophilite solubility products, and run products of fluid-melt interaction and dissolution, repeat, and crystallization experiments

Experiment name	*T* final (°C)	*P* (MPa)	*d* (days)	*ASI*	ASI_{Li}	MnO (wt %)	Ta_2O_5 (wt%)	Nb_2O_5 (wt%)	Li_2O (wt%)	B_2O_3 (wt%)	P_2O_5 (wt%)	$logK_{sp}^{col}$ (mol^2/kg^2)	$logK_{sp}^{lth}$ (mol^3/kg^3)	Run products
Metasomatic experiments														
SMn1Nb5000-700	700	200	5	1.08	0.92	0.39(±0.03)	-	0.58(±0.06)	0.82(±0.07)	1.42(±0.06)	1.28(±0.07)	-2.92(±0.02)	-3.47(±0.01)	gl,col,lth
SMn1Nb5000-675	675	200	5	1.07	0.91	0.25(±0.07)	-	0.54(±0.07)	0.77(±0.08)	1.82(±0.12)	1.21(±0.17)	-3.15(±0.04)	-3.71(±0.03)	gl,col,lth,ano
SMn1Nb5000-650	650	200	5	1.08	0.93	0.21(±0.02)	-	0.56(±0.06)	0.71(±0.03)	1.91(±0.06)	1.08(±0.26)	-3.21(±0.02)	-3.87(±0.02)	gl,col,lth,ano
SMn1Ta5000-700	700	200	5	1.08	0.92	0.43(±0.14)	0.62(±0.06)	-	0.77(±0.05)	1.39(±0.09)	1.21(±0.17)	-	-3.48(±0.04)	gl,lth
SMn1Ta5000-650	650	200	5	1.09	0.94	0.26(±0.07)	0.94(±0.14)	-	0.67(±0.05)	1.94(±0.15)	1.02(±0.26)	-	-3.83(±0.04)	gl,lth,ano,mic
Dissolution, repeat, and crystallization experiments														
COL-850-1	850	200	5	1.03	0.84	0.52(±0.02)	-	1.98(±0.09)	1.05(±0.01)	2.36(±0.02)	1.47(±0.08)	-2.26(±0.01)	-	gl, col
COL-800	800	200	5	1.02	0.83	0.40(±0.03)	-	1.46(±0.08)	1.05(±0.01)	2.36(±0.02)	1.44(±0.08)	-2.51(±0.02)	-	gl, col
COL-800-2 $_{rep}$	800	200	5	1.04	0.85	0.40(±0.02)	-	1.53(±0.08)	1.05(±0.01)	2.36(±0.02)	1.50(±0.09)	-2.48(±0.01)	-	gl, col
COL-750	750	200	5	1.04	0.85	0.33(±0.02)	-	1.21(±0.08)	1.05(±0.01)	2.36(±0.02)	1.48(±0.09)	-2.68(±0.01)	-	gl, col
COL-700	700	200	5	1.04	0.85	0.25(±0.02)	-	0.94(±0.06)	1.05(±0.01)	2.36(±0.02)	1.44(±0.08)	-2.90(±0.02)	-	gl, col
COL-700C-1 $_{xl}$	700	200	10	1.04	0.85	0.26(±0.02)	-	0.94(±0.06)	1.05(±0.01)	2.36(±0.02)	1.48(±0.07)	-2.89(±0.01)	-	gl, col

Notes: The initial ASI is the molar Al/(Na+K) of the starting composition, which is 1.00 for the dissolution, repeat and crystallization experiments and 1.01 to 1.02 for the metasomatic experiments; *T* temperature; *P* pressure; *d* duration; *ASI* molar Al/(Na+K) of run product; ASI_{Li} molar Al/(Na+K+Li) of run product; $logK_{sp}^{col}$ columbite solubility product; $logK_{sp}^{lth}$ lithiophilite solubility product; 1σ standard deviation are in parentheses and are calculated as an average of 20 spot analyses; weight percent values are averages of 20 spot analyses (EPMA) for all except for Li_2O and B_2O_3 for metasomatic experiments, which are averages of 4-6 SIMS analyses; Li_2O and B_2O_3 were not determined for dissolution, repeat and crystallization experiments (values are from bulk starting glass) as they are assumed to be unchanged because there was no hydrothermal fluid present to remove these elements from the melt; *gl* glass; *col* columbite; *mic* microlite; *lth* lithiophilite; *ano* anorthoclase; *rep* repeat experiment; *xl* crystallization experiment.

This is a preprint, the final version is subject to change, of the American Mineralogist (MSA)
Cite as Authors (Year) Title. American Mineralogist, in press.
DOI: https://doi.org/10.2138/am-2020-7216

780 Table 5. FE-EPMA-WDS analyses of columbite-(Mn) from fluid-melt interaction experiments

781

Experiment name and grain analyzed	SiO_2* (Mass%)	P_2O_5* (Mass%)	MnO (Mass%)	Nb_2O_5 (Mass%)	Total (Mass%)	Total MnO+Nb_2O_5	Chemical Formula
SMn1Nb5000-675_COL_1	4.19	0.51	19.23	72.59	96.52	91.82	$Mn_{0.99}Nb_{2.00}O_6$
SMn1Nb5000-675_COL_1b	3.37	0.11	19.08	74.28	96.84	93.36	$Mn_{0.97}Nb_{2.01}O_6$
SMn1Nb5000-675_COL_1c	3.19	0.11	19.37	74.52	97.19	93.89	$Mn_{0.98}Nb_{2.01}O_6$
SMn1Nb5000-675_COL_1d	2.75	0.11	19.50	75.54	97.89	95.04	$Mn_{0.97}Nb_{2.01}O_6$
SMn1Nb5000-675_COL_1e	2.81	0.11	19.23	75.52	97.68	94.75	$Mn_{0.96}Nb_{2.02}O_6$
SMn1Nb5000-675_COL_1f	4.88	0.12	18.80	71.65	95.45	90.45	$Mn_{0.98}Nb_{2.01}O_6$
SMn1Nb5000-675_COL_2	5.09	0.13	19.44	73.41	98.07	92.85	$Mn_{0.99}Nb_{2.00}O_6$
SMn1Nb5000-675_COL_3	3.18	1.22	19.71	73.09	97.19	92.80	$Mn_{1.01}Nb_{2.00}O_6$
SMn1Nb5000-675_COL_4	7.03	0.16	18.91	70.66	96.75	89.57	$Mn_{1.00}Nb_{2.00}O_6$
SMn1Nb5000-675_COL_5	3.37	1.98	20.29	71.87	97.52	92.17	$Mn_{1.05}Nb_{1.98}O_6$
SMn1Nb5000-675_COL_6	6.56	0.18	19.08	71.31	97.13	90.39	$Mn_{1.00}Nb_{2.00}O_6$
SMn1Nb5000-675_COL_7	4.24	0.39	19.37	75.62	99.63	94.99	$Mn_{0.97}Nb_{2.01}O_6$
SMn1Nb5000-650_COL_1	4.48	3.46	20.00	68.36	96.30	88.36	$Mn_{1.07}Nb_{1.97}O_6$
SMn1Nb5000-650_COL_2	2.60	1.30	19.63	70.90	94.44	90.53	$Mn_{1.03}Nb_{1.99}O_6$
SMn1Nb5000-650_COL_3	9.12	0.21	18.72	69.19	97.24	87.91	$Mn_{1.01}Nb_{2.00}O_6$
SMn1Nb5000-650_COL_4	1.14	0.22	19.65	77.25	98.26	96.90	$Mn_{0.96}Nb_{2.02}O_6$
SMn1Nb5000-650_COL_5	6.71	3.21	19.53	64.97	94.41	84.50	$Mn_{1.10}Nb_{1.96}O_6$
SMn1Nb5000-700_COL_1	4.71	0.11	19.17	73.28	97.28	92.46	$Mn_{0.98}Nb_{2.01}O_6$
SMn1Nb5000-700_COL_1b	4.03	0.11	19.64	75.26	99.04	94.90	$Mn_{0.98}Nb_{2.01}O_6$
SMn1Nb5000-700_COL_1c	13.55	0.26	17.15	62.46	93.41	79.61	$Mn_{1.02}Nb_{1.99}O_6$
SMn1Nb5000-700_COL_2	11.72	0.25	17.58	64.21	93.76	81.79	$Mn_{1.02}Nb_{1.99}O_6$
SMn1Nb5000-700_COL_3	0.62	1.05	20.11	75.49	97.27	95.60	$Mn_{1.00}Nb_{2.00}O_6$
SMn1Nb5000-700_COL_4	2.71	0.07	19.87	75.69	98.34	95.56	$Mn_{0.99}Nb_{2.00}O_6$
SMn1Nb5000-700_COL_5	6.96	0.18	18.92	71.22	97.28	90.14	$Mn_{1.00}Nb_{2.00}O_6$
SMn1Nb5000-700_COL_6	4.61	2.44	20.29	70.24	97.58	90.52	$Mn_{1.07}Nb_{1.97}O_6$
SMn1Nb5000-700_COL_7	2.51	0.06	19.72	76.72	99.00	96.44	$Mn_{0.97}Nb_{2.01}O_6$
SMn1Nb5000-700_COL_8	3.07	0.23	19.78	75.65	98.73	95.43	$Mn_{0.98}Nb_{2.01}O_6$
SMn1Nb5000-700_COL_9	2.99	0.08	19.86	76.27	99.19	96.12	$Mn_{0.98}Nb_{2.01}O_6$
Average concentrations	**4.72**	**0.66**	**19.34**	**72.40**	**97.12**	**91.74**	**$Mn_{1.00}Nb_{2.00}O_6$**

* SiO_2 and P_2O_5 were analyzed to determine approximate glass contribution to analysis as grains were typically <1 µm wide. High SiO_2 and P_2O_5 values represent background analysis of either the glass or lithiophilite grains where the columbite-(Mn) grain was smaller than the beam size (approx. 1 µm).

782

783

784

785 Table 6. Enthalpy of formation and dissolution for columbite-(Mn) from this and comparable
786 previous studies, and enthalpy of formation for lithiophilite.

Mineral	Slope ($dlogK_{sp}/d(1000/T)$)	$\Delta H_{form\ or\ diss}$ (kJ/mol)
Columbite-(Mn) dissolution experiments	-4.49 (±0.18)	86.0 (±3.4)
Columbite-(Mn) fluid-melt interaction experiments	-5.08 (±1.80)	97.3 (±34.5)
Columbite-(Mn) dissolution (Aseri et al. 2015)	-	117.1 (±1.4)
Columbite-(Mn) dissolution (Fiege et al. 2018)	-	118.0 (±22.9)
Lithiophilite	-7.26 (±0.99)	139.0 (±19.0)

787

788 **Figure Captions**

789 Figure 1. Back scattered electron image of part of fluid-melt interaction experiment
790 SMn1Nb5000-650 (1 wt% Mn fluid, 5000 ppm Nb glass at 650 °C, 200 MPa, 5 days) with
791 representative phases labelled columbite-(Mn) [col], lithiophilite [lth], anorthoclase [ano] and
792 glass [gl].

793

794 Figure 2. Back scattered electron image of part of fluid-melt interaction experiment
795 SMn1Ta5000-650 (1 wt% Mn fluid, 5000 ppm Ta glass at 650 °C, 200 MPa, 5 days) with
796 representative phases labelled Ca-Ta oxide, lithiophilite [lth], anorthoclase [ano] and glass [gl].

797

798 Figure 3. Back scattered electron image of part of fluid-melt interaction experiment
799 SMn1Nb5000-700 (1 wt% Mn fluid, 5000 ppm Nb glass at 700 °C, 200 MPa, 5 days) with
800 representative phases labelled columbite-(Mn) [col], lithiophilite [lth], and glass [gl].

801

802 Figure 4. $logK_{sp}$ vs 1000/T for columbite-(Mn) and lithiophilite from all experiments. Error bars
803 are ± 1 σ and in most instances are smaller than the data point.

This is a preprint, the final version is subject to change, of the American Mineralogist (MSA)
Cite as Authors (Year) Title. American Mineralogist, in press.
DOI: https://doi.org/10.2138/am-2020-7216

Figure 1

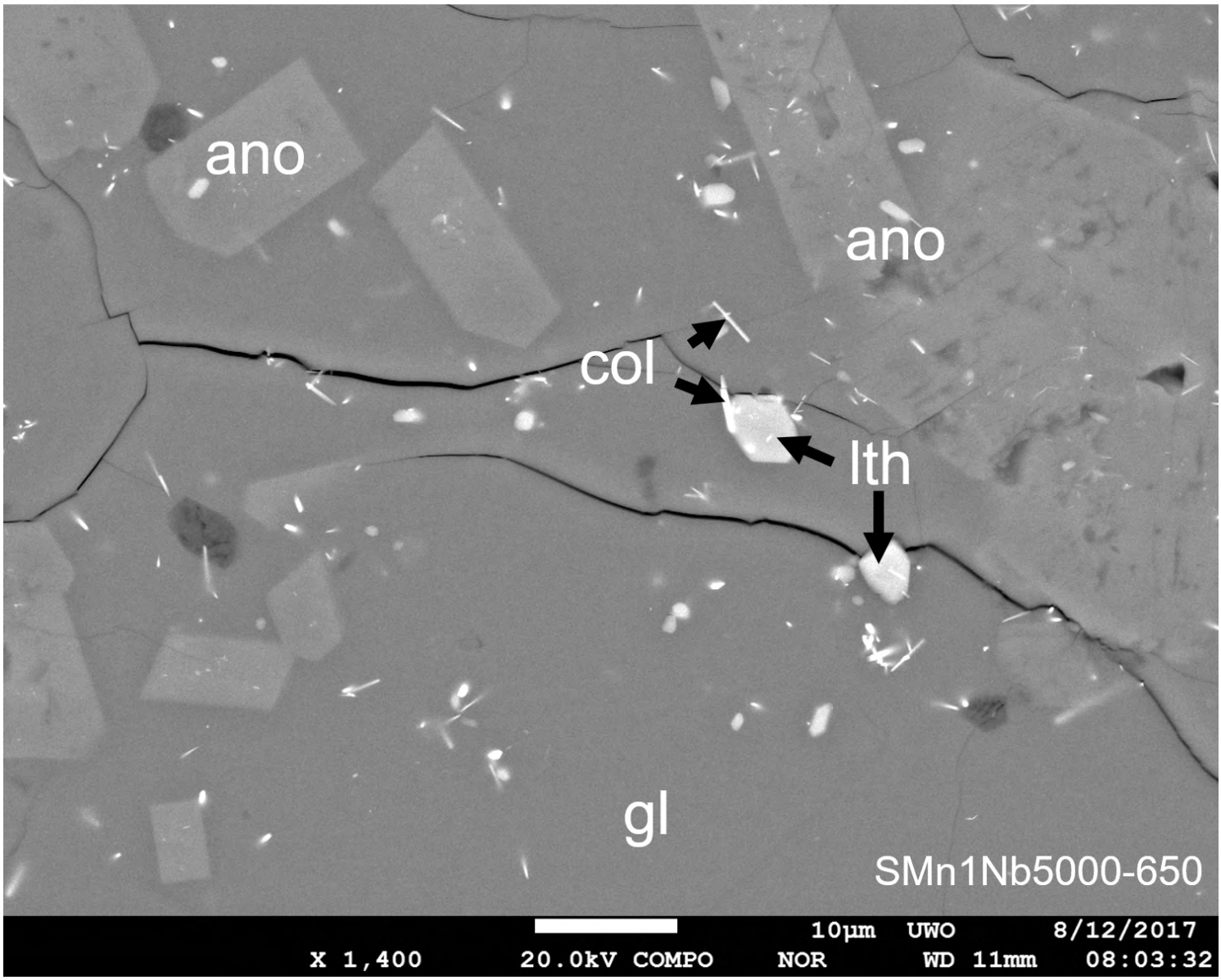

This is a preprint, the final version is subject to change, of the American Mineralogist (MSA)
Cite as Authors (Year) Title. American Mineralogist, in press.
DOI: https://doi.org/10.2138/am-2020-7216

Figure 2

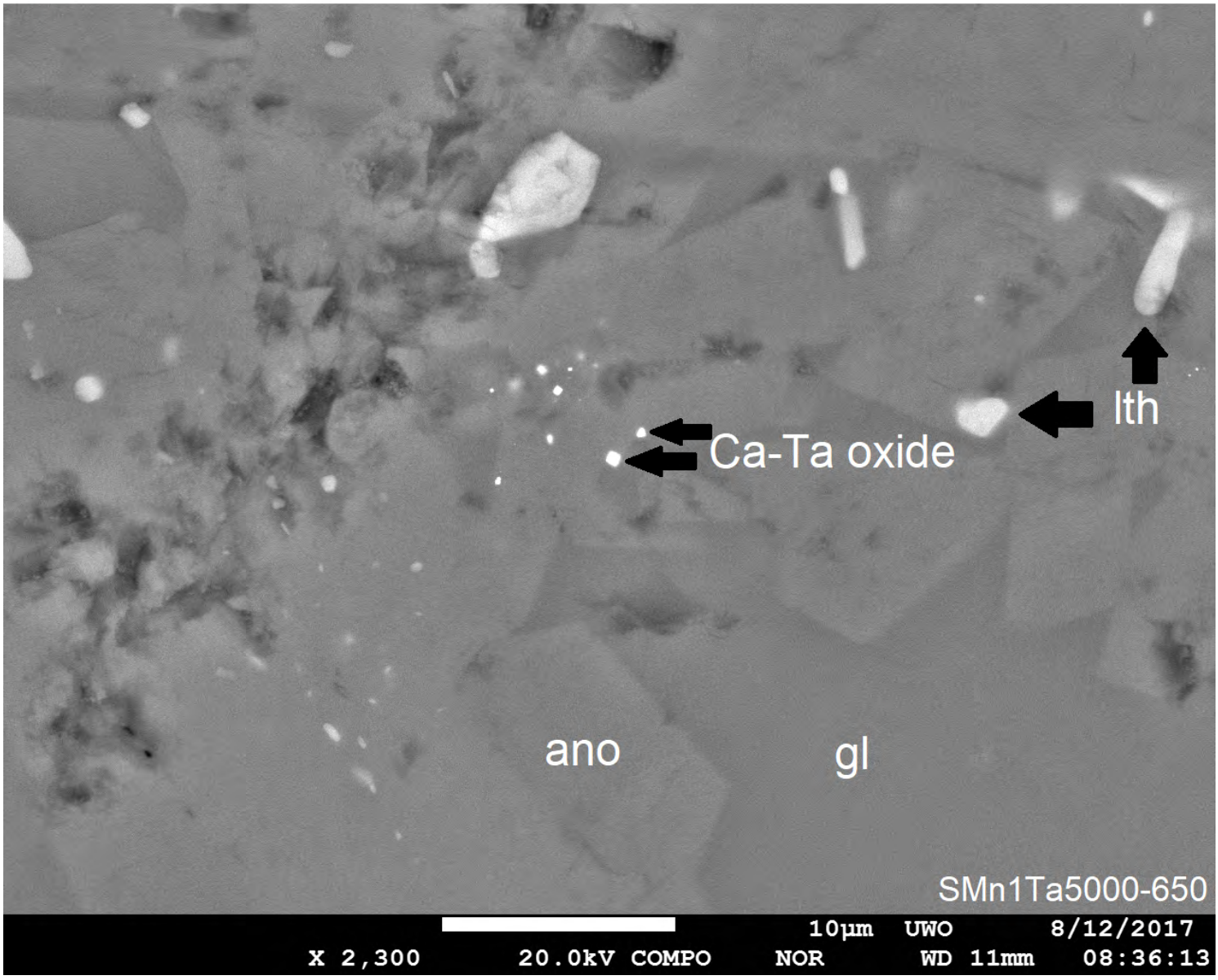

This is a preprint, the final version is subject to change, of the American Mineralogist (MSA)
Cite as Authors (Year) Title. American Mineralogist, in press.
DOI: https://doi.org/10.2138/am-2020-7216

Figure 3

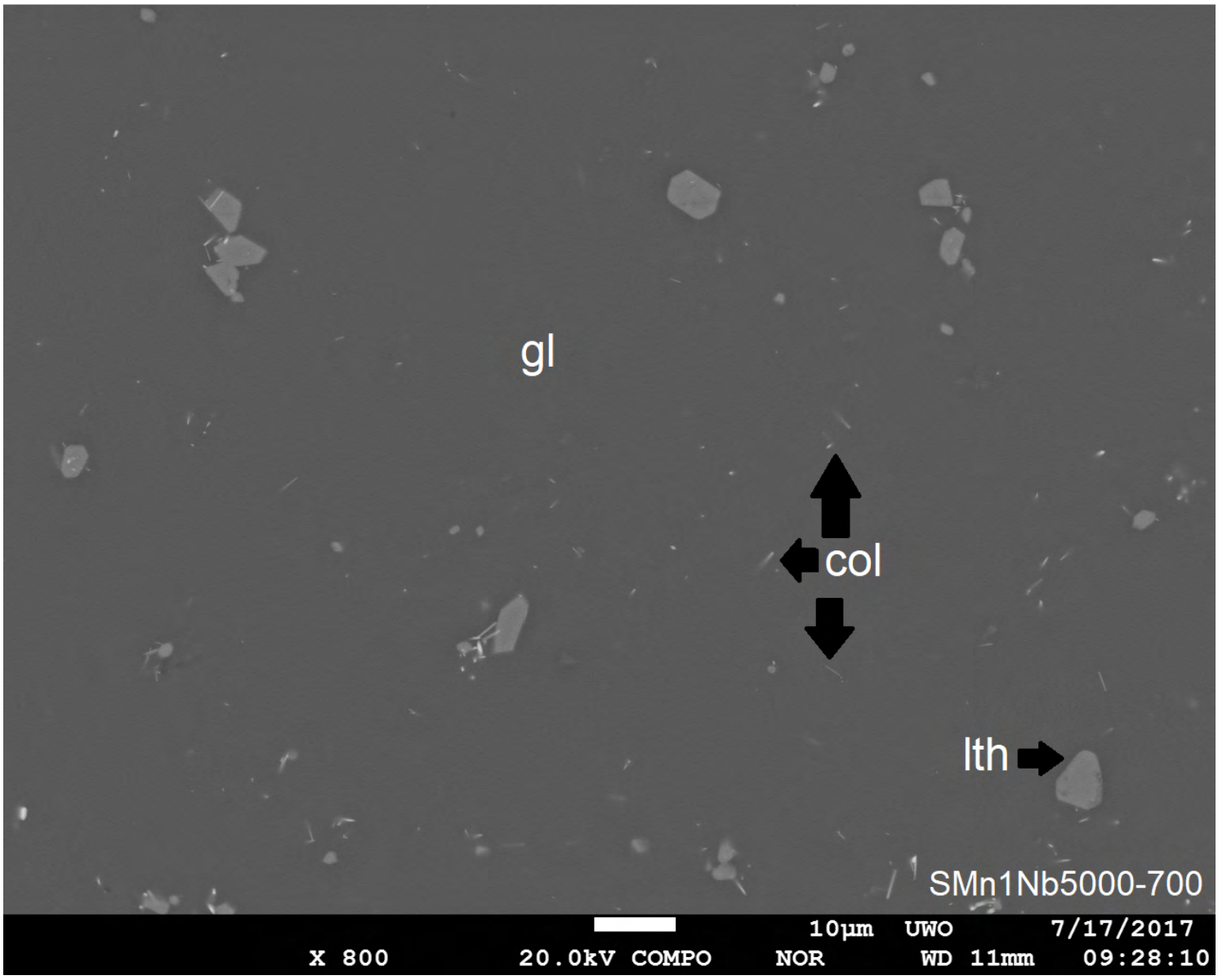

This is a preprint, the final version is subject to change, of the American Mineralogist (MSA)
Cite as Authors (Year) Title. American Mineralogist, in press.
DOI: https://doi.org/10.2138/am-2020-7216

Figure 4